Title
A TIME-ZERO DETECTOR UTILIZING ISOCHRONOUS TRANSPORT OF SECONDARY ELECTRONS

Author
Zebelman, A.M.

Publication Date
1976-10-01

Submitted to Nuclear Instruments and Methods

LBL-5095
Preprint c.1

A TIME-ZERO DETECTOR UTILIZING ISOCHRONOUS TRANSPORT OF SECONDARY ELECTRONS

A. M. Zebelman, W. G. Meyer, K. Halbach,
A. M. Poskanzer, R. G. Sextro, G. Gabor, and D. A. Landis

October 14, 1976

Prepared for the U. S. Energy Research and Development Administration under Contract W-7405-ENG-48

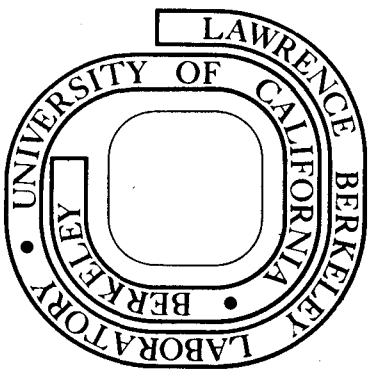

DISCLAIMER

LBL-5095

A TIME ZERO DETECTOR UTILIZING ISOCHRONOUS TRANSPORT OF SECONDARY ELECTRONS

A. M. Zebelman, W. G. Meyer, K. Halbach, A. M. Poskanzer,

R. G. Sextro, G. Gabor and D. A. Landis

October 1976

LBL-5095

A TIME-ZERO DETECTOR UTILIZING ISOCHRONOUS TRANSPORT OF SECONDARY ELECTRONS*

A. M. Zebelman,† W. G. Meyer, K. Halbach, A. M. Poskanzer, R. G. Sextro, G. Gabor and D. A. Landis

Lawrence Berkeley Laboratory
University of California
Berkeley, California 94720

14 October 1976

Abstract

A time-zero detector has been developed for use in reaction product mass identification which has as its novel feature a 180° isochronous transport of secondary electrons in a magnetic field. The secondary electrons produced when particles pass through a thin carbon foil are accelerated to approximately two keV by a parallel-wire harp of 99% transmission. The accelerated electrons are then transported 180° in a uniform magnetic field of 80 gauss containing a collimator placed at the 90° position. A background suppression grid is placed just in front of the electron detector which is comprised of two microchannel plates in series acting as an electron multiplier. The device allows placement of the thin foil perpendicular to the fragment flight path and permits shielding of the electron detector from the beam and reaction products while using only modest accelerating voltages. The time-of-flight resolutions measured between this timing detector and a 120 μm silicon detector when using 104 MeV ^{16}O ions and 8.78 MeV alpha particles were 90 and 150 psec, respectively (full widths at half maxima).

---

*This work was done with support from the U.S. Energy Research and Development Administration.

†Present temporary address: Department of Laboratory Medicine, University Hospital, University of Washington, Seattle, Wash. 98195.

Secondary electron emission from thin foils has long been used as a timing device in time-of-flight mass identification of nuclear fragments. It is especially useful for the time-zero signal because the thin foil causes a minimal degradation of the velocity of the fragments. In previous work the foil was mounted at 45° to the path of the fragments with the electrons collected perpendicular to the face of the foil, or alternatively, the foil was mounted perpendicular to the path of the fragments and the electrons were collected on a detector off to the side, out of the path of the fragments. With modern fast electronics and electron detector systems capable of time resolutions of the order of 100 psec, neither method is satisfactory. Because of the short flight paths now used the first method,[1-9] with the foil at 45°, leads to a significant dispersion in fragment flight distances. Placing the stop detector also at 45° is of little help for large solid angle systems where the fragments are diverging from a target.[10] In the second method, with the foil perpendicular to the flight path, electron transport is achieved using either electrostatic lenses,[11-13] or electrostatic [1,7] or magnetic deflection.[4] The dispersion in electron collection times is usually significant but has sometimes been minimized by the use of large electron collection voltages[2,4,6,7,12] of 12 to 24 kV. These voltages were often also needed because of the electron detectors employed.

Ideally an isochronous transport system for the secondary electrons is required which allows the foil to remain perpendicular to the fragment path and the detector to be placed in a location shielded from the beam. Our solution to the problem is a 180° bend in a homogeneous magnetic field as shown in Fig. 1. It is well known from the principle of the

cyclotron that such a bend is isochronous both with respect to position and energy. There is also a one-to-one focus with respect to position and initial angle. However, the flight time depends on the initial angle in the plane of the bend as seen in Fig. 1. The secondary electrons are emitted with a large angular spread but with energies of the order of only a few electron volts. We accelerate them to two keV, thereby greatly reducing their angular dispersion. The acceleration is accomplished with a high transmission wire harp oriented so that the individual wires are parallel to the plane of the 180° bend. Thus the nonuniform electric field due to the spacing of the wires does not introduce angular dispersion in the plane of the bend, thereby preserving the time resolution. In the lateral direction the nonuniform accelerating field spreads the image somewhat, but to first order does not introduce any time dispersion. Finally, any residual angular dispersion in the plane of the bend is reduced by the use of a collimator located at the 90° position of the bend. Such quarter-turn collimators have also been used in cyclotrons. As seen in Fig. 1, at the position of such a collimator, the normal trajectories which have equal path length, cross over, while any remaining off-angle rays hit the collimator.

In the first model constructed of this device a small satellite peak appeared in the time spectrum a few nsec later than the main peak. This problem was traced to the secondary electrons hitting the insensitive contact surface of the microchannel plate where they produced tertiary electrons which then executed a small 180° loop hitting the channel plate again, and thus produced a delayed signal. This problem was solved and the background of the device was further reduced by

placing a suppression grid in front of the channel plate.

In summary we have produced an isochronous secondary-electron transport system which allows the foil to be perpendicular to the path of the fragments and the detector to be shielded. In other devices[8,9] in which the detector views the foil directly, x-rays may cause the detector signal to rise too soon. Also, our device preserves the position information by producing a one-to-one image of the foil. Although it is not further discussed in this article it should be possible to obtain position information by replacing the anode with a position sensitive detector, while obtaining time information of somewhat reduced quality from the back surface of the channel plate.

Handy Equations

For the design of such a device it is useful to have at hand some simple equations describing the non-relativistic behavior of electrons in electric and magnetic fields. In presenting these equations we will use the units: cm, volt, gauss, nsec, and radians.

The time of flight (t) over a distance (d) in a field-free region after acceleration by a voltage (V) is

$$t = 16.8\ d/\sqrt{V} \quad . \tag{1}$$

The time of flight when starting from rest in a uniform electric field (V/d) is

$$t = 33.7\ d/\sqrt{V} \quad . \tag{2}$$

The radius of curvature (ρ) in a uniform magnetic field (H) is

$$\rho = 3.38\ \sqrt{V}/H \quad , \tag{3}$$

and the time of flight for a 180° bend is

$$t = 179/H \quad . \tag{4}$$

The trajectory equations for electrons starting from rest in crossed electric and magnetic fields will also be needed. It is assumed that the electric field (E) is in the negative x direction and the magnetic field in the z direction. Then,

$$x = (Ec/\omega H)(1-\cos \omega t) \tag{5a}$$

$$y = (Ec/\omega H)(\omega t-\sin \omega t) \quad , \tag{5b}$$

where the cyclotron frequency, $\omega = 1.76 \times 10^{-2}$ H and Ec = V/10d (in stat-volts/nsec). The angle (θ) between the trajectory and the x direction is

$$\theta = \omega t/2 \quad . \tag{6}$$

When an electron enters a uniform magnetic field region containing no electric field at an angle θ to the x direction, the maximum x value obtained is

$$x_{max} = \rho(1 - \sin \theta), \tag{7}$$

and the time of flight needed to return to the plane of entry is

$$t = (179/H)(1-2\ \theta/\pi) \quad . \tag{8}$$

It follows that

$$|\Delta t/\Delta\theta| = 114/H. \tag{9}$$

Design Criteria

The smallest channel plate available had a diameter of 2.5 cm with an active area diameter of 1.8 cm. In order to keep the device compact the radius of curvature was chosen to be 2 cm, thus separating the centers of the foil and channel plate by 4 cm. The magnet gap was made just big enough to hold the channel plates, their mounting flange, and the high voltage insulators. The pole tips were then made big enough to give a homogeneous field in the region containing the electron trajectories, allowing one-half the gap size on the sides. A desire to use a modest acceleration voltage of about two kV then determined the desired magnetic field. These and other design parameters are given in Table I. A scale drawing of the mechanical arrangement is shown in Fig. 2.

An electrical schematic is shown in Fig. 3. The anode is at ground potential. Two negative high voltage supplies are needed, one for the channel plates and one to provide the acceleration voltage. As will be shown in the next section, the suppression grid can have a wide range of voltages more positive than the front face of the first channel plate, and therefore was tied to the back of this channel plate. The suppression grid and acceleration harp are part of the Faraday cage forming an electrostatic field-free region for most of the electron transport. The high voltage supply for the carbon foil is more negative than the acceleration harp and is adjusted for maximum transport efficiency as described below. With the divider chain network shown, the Faraday cage voltage is 61% of the channel plate voltage supply. Therefore the acceleration voltage between the carbon foil and harp is equal to the foil voltage minus 61% of the channel plate voltage.

The design of the quarter-turn collimator which is summarized in Table I required some care. Because the acceleration region has crossed electric and magnetic fields the electrons have already begun to bend when they enter the Faraday cage. Therefore the center of the collimator was placed at a position equal to slightly less than the radius of curvature. The radial size of the opening in the collimator was chosen to determine the angular acceptance and therefore the time spread acceptance.

Performance

All performance tests made with the time-zero detector were carried out utilizing the electronic configuration shown in Fig. 4. The rise time from the channel plate anode was about 0.5 nsec. The fast amplifier had a rise time of about 0.8 nsec and the constant fraction discriminator had the clipping time adjusted to minimize electronic "walk" with pulse height. The channel plate pulse height was recorded using a 20 nsec-wide linear gate followed by a stretcher.

In order to determine the optimum operating voltage of the electron transport device, measurements were made of the efficiency as a function of acceleration voltage. Figure 5 shows these efficiency curves measured with and without the quarter-turn collimator. It can be seen that the presence of the quarter-turn collimator considerably decreased the width of the curve, but reduced the efficiency at the operating voltage by only 10%. The decrease in width is because the collimator selects electron energies after acceleration as well as angles.

In the initial construction of this detector small satellite peaks occurred 2 to 3 nsec (and multiples of this time) later than the main

peak when performing time-of-flight measurements of monoenergetic particles. Tests showed that the satellite peaks came from tertiary electrons which were produced when the accelerated secondary electrons from the carbon foil collided with the inactive contact surface of the channel plate. These low-energy tertiary electrons then executed small semicircular orbits, because of the magnetic field, into active multiplying channels of the channel plate. The channel-plate pulse height spectrum associated with the satellite peak fell off more steeply with pulse height than did the main peak. Raising the discriminator would reduce the effect but at the expense of efficiency. Instead, to eliminate the satellite peaks a suppression grid was placed in front of the channel plate to accelerate any tertiary electrons away from the channel plate and into the surrounding walls. Measurements were made as a function of suppression voltage to determine the voltage needed to completely eliminate the satellite peaks. These are shown in Fig. 6. The peaks became sharper with increasing voltage because of the decreased angular spread. The shifts in time are more complicated to understand. With zero suppression voltage the peak was at about the normal transport time, which is independent of electron energy, of 2.2 nsec listed in Table I. With 10 volts the trajectories do not penetrate the suppression grid so that the electrons spend all their time in the crossed-field region where the transport times are quite long as calculated by equation 5a. At the higher voltages the electrons penetrate the grid and both equations 5a and 8 must be used to calculate the total transport times. At 40 and 110 volts the times are 2.8 and 2.6 nsec respectively, which are not far from the peaks in Fig. 6. It was

found that a suppression voltage greater than 210 volts was required to completely eliminate the satellite peaks as shown in Fig. 7. The decrease in efficiency shown in Fig. 7 was mostly accounted for by the disappearance of the satellite peaks. Since the only small additional decrease occurred between 250 and 1000 volts, it was decided, for convenience, to use 900 volts. This voltage was available in the voltage divider chain. As a result of this decision the carbon foil voltage was lowered by this amount and the channel plate became shielded from background electrons by this voltage. Also the electrons impinging on the channel plate have slightly higher efficiency at this lower voltage.

Studies were made using 8.78 MeV alpha particles to optimize certain design parameters. The parameters studied were: 1) the strength of the magnetic field, 2) the use of the quarter-turn collimator, and 3) the use of the parallel-wire acceleration harp instead of a square mesh grid. The different configurations tested and the time resolution determined for each are given in Table 2. It can be seen that the use of the higher magnetic field, and either the quarter-turn collimator, or the acceleration harp were necessary to optimize the timing resolution of the detector. Both may be necessary when the resolution is improved further.

The performance of this time-zero detector was tested with heavy ions at the 88" cyclotron. Time-of-flight measurements were made using a 120 μm Si stop detector. The bias voltage of the fully depleted Si detector was chosen to give a minimum field of 2 volts/μm in the silicon.

The channel plate pulse-height spectra obtained for 104 MeV ^{16}O ions and 8.78 MeV alpha particles are shown in Fig. 8. The differences in the shapes and the peak positions for the two reflect the difference in the average number of secondary electrons produced in the carbon foil. The results of the resolution tests are tabulated in Table 3, and time spectra are shown in Figs. 9(a) and 9(b). The differences in detection efficiencies for ^{4}He and ^{16}O ions are due to the higher yield of secondary electrons produced by the ^{16}O ions.

In conjunction with the development of the present device we also tested a time-zero detector[8,9] which placed the foil at 45° with no magnetic transport. The results for 60 MeV ^{16}O with a 127 μm E detector (biased to give a minimum field of 2 volts/μm) are shown in Table 4.

Since our early work[14] with a silicon ΔE detector in a ΔE-E-TOF system, techniques have steadily improved.[15-17] Our present results for 60 MeV ^{16}O ions incident on a telescope consisting of a 19 μm ΔE (biased to give a minimum field of 2.5 volts/μm) and a 127 μm E (2 volts/μm) are also shown in Fig. 9(c) and Table 4. From Table 4 it can be seen that the performance of the present time-zero detector is comparable with other fast timing devices. It should be pointed out that the present device has the advantages of: 1) minimum energy degradation of detected particle, 2) use over a very large range of masses and energies, 3) compactness and 4) optimum detector shielding from stray radiation.

Suggested Improvements

The conical anode was shaped to have an impedance of 50 ohms and therefore reduce electrical reflections. If ringing is not going to be a problem, then the anode could be simply a flat plate. This would make more efficient use of the active area of the channel plate and allow a still more compact design, since the magnet could be made smaller. However, care must be taken that the variation in signal transport time across the plate does not contribute significantly to the time spread.

The rectangular slit in the quarter-turn collimator should actually be shaped like the arc of a circle. The length of the arc should be designed so that this second order effect is no larger than the first order effect due to the radial height of the slit.

If background is a problem, the shielding of the channel plate detector could be considerably improved. Essentially one could enclose it in a small box with pump-out baffles so that the only direct access is the slit of the quarter-turn collimator through which the electrons enter. At present the channel plates are sensitive to a nearby ionization gauge. Better shielding would also cure this problem.

Construction Details

The magnet was constructed of two pieces of 3/16 inch cold rolled steel joined at the top and bottom (by means of epoxy) with three Alnico V steel magnet bars. The Alnico V bars were purchased slightly longer than desired and were ground to the dimensions required. The 80 gauss magnetic field was formed by placing the magnet in the field

of a large dipole electronmagnet. The magnet was first saturated by raising the field to several hundred gauss, and then the field was reversed until, by trial and error the desired field and field uniformity were obtained. The inside walls of the magnet were electrically insulated from the mounting block by epoxying thin sheets of Nema G-10 epoxy glass to the four surfaces.

The mounting block was made out of two 1/2 inch thick pieces of Nema G-10 epoxied together because one piece large enough was not available. A thin piece of Nema G-10 with one copper-clad surface (standard printed circuit board material) was epoxied onto one surface of the block to serve as one side of the Faraday cage. Two large holes were bored in the block to accommodate the carbon foil/acceleration harp and the channel plate/suppression grid assemblies.

The carbon foil/acceleration harp assembly was constructed of a copper ring, an aluminum foil holder, a Teflon insulator, and a copper mounting flange for the stainless steel harp. Commercially available carbon foils (10-20 $\mu g/cm^2$) were floated and picked up on the aluminum holders and then laminated with a few $\mu g/cm^2$ of Formvar for added rigidity. The copper ring, foil holder and insulator were sandwiched together and set into the mounting block. The assembly was held in place by the harp mounting flange which was screwed to the copper-clad surface of the mounting block. High voltage was supplied to the carbon foil by a lead to the copper ring brought through a small diameter hole drilled into the mounting block. The acceleration harp was constructed by attaching 0.001 inch stainless steel wires at one mm spacing to the copper flange by means of electrically-conducting epoxy.

The quarter-turn collimator was constructed of aluminum and attached to the copper-clad surface of the mounting block with screws.

The channel plate/suppression grid assembly consisted of a brass anode cone, two Varian 8900 series microchannel plates in a Chevron arrangement, and a copper Electromesh suppression grid (96% transmission) which was attached to a copper mounting flange by means of electrically conducting epoxy. The surface of the anode was coated with carbon black to suppress secondary electron emission. Voltages from the divider chain were applied to the front and rear surfaces of each channel plate and to the suppression grid by means of 0.0005 inch copper foils which were cut so that they only made contact with the conducting surface of the channel plates and the suppression grid mounting flange. The copper foils for the back of the first channel plate and the front of the second plate were electrically insulated from each other by means of a 0.002 inch thick Mylar film. The suppression grid and the front of the first channel plate were electrically insulated by a 1/16 inch thick Nema G-10 spacer. The anode was set in a conically shaped shield with a flange whose inner diameter was slightly smaller than the diameter of the channel plates. The channel plate package was held together by carefully sandwiching it between the suppression grid mounting flange and the flange of the anode shield. The two flanges were held together with four Nylon screws. The suppression grid mounting flange was then screwed to the copper-clad surface of the mounting block.

Five sides of the Faraday cage (the sixth side being the copper-clad surface of the mounting block) were constructed of copper wire cloth (normal household screen material). A circular hole was cut out

of the mesh on line with the carbon foil to leave the fragment flight path unobstructed. The acceleration harp, the suppression grid, and Faraday cage are all at the same electrical potential.

The voltage divider chain was made up of four temperature-insensitive 1/8 watt metal film resistors cemented with heat-conducting epoxy into a brass tube which was put in thermal contact with the scattering chamber. To minimize problems from electrical breakdown, a one megohm current-limiting resistor was placed in series between the voltage divider chain and its high voltage power supply.

Acknowledgements

The authors wish to express their grateful appreciation to D. J. Vieira, F. S. Goulding, C. E. Hartsock, M. Maier, G. D. Westfall, W. S. Cooper, and M. Zisman for their help in different phases of this work.

References

1) V. T. Grachev, B. V. Grigor'ev, G. A. Korolev, D. M. Seliverstov, and A. P. Shesternev, Bull. Acad. Sci. USSR, Phys. Ser. 32 (1968) 653

2) E. Dietz, R. Bass, A. Reiter, U. Friedland, and B. Hubert, Nucl. Instr. and Methods 97 (1971) 581

3) W. Pfeffer, B. Kohlmeyer, and W.F.W. Schneider, Nucl. Instr. and Methods 107 (1973) 121

4) E. Dietz, J. V. Czarnecki, W. Patscher, W. Schäfer, and R. Bass, Nucl. Instr. and Methods 108 (1973) 607

5) E. Andrade, I. Alvarez, and C. Cisneros de Alvarez, Nucl. Instr. and Methods 121 (1974) 359

6) M. Fluss, S. Kaufman, E. Steinberg, and B. Wilkins, Private Communication (1974)

7) W. Lang and H.-G. Clerc, Nucl. Instr. and Methods 126 (1975) 535

8) G. Gabor in F. S. Goulding and B. G. Harvey, Ann. Rev. Nucl. Science 25 (1975) 203

9) G. Gabor, W. Schimmerling, D. Greiner, F. Bieser, and P. Lindstrom, Nucl. Instr. and Methods 130 (1975) 65.

10) A solution to this problem is to use two 45° foils perpendicular to each other and to average the two time signals, W.F.W. Schneider, private communcation (1975)

11) W.F.W. Schneider, B. Kohlmeyer, and R. Bock, Nucl. Instr. and Methods 87 (1970) 253

12) H.-G. Clerc, H. J. Gehrhardt, L. Richter, and K. H. Schmidt, Nucl. Instr. and Methods 113 (1973) 325

13) V.F.W. Schneider, B. Kohlmeyer, W. Pfeffer, F. Pühlhofer, and R. Bock, Nucl. Instr. and Methods 123 (1975) 93

14) G.W. Butler, A. M. Poskanzer, and D. A. Landis, Nucl. Instr. and Methods 89 (1970) 189

15) H. Pleyer, B. Kohlmeyer, W. F. Schneider, and R. Bock, Nucl. Instr. and Methods 96 (1971) 263

16) J. D. Bowman, A. M. Poskanzer, R. G. Korteling, and G. W. Butler, Phys. Rev. C. 9 (1974) 836

17) B. Zeidman, W. Henning, and D. G. Kovar, Nucl. Instr. and Methods 118 (1974) 361

Table 1. Design Parameters

Magnet		
radius of curvature ρ	2.0	cm
field H	80	gauss
pole tips	6 × 10	cm
gap	4.0	cm
Acceleration Voltage V (Eq. 3)	2240	volts
Approx. time of flight t (Eq. 4)	2.2	nsec
Acceleration Region		
carbon foil diameter	1.3	cm
foil-harp separation d	0.28	cm
time of acceleration t (Eqs. 5a or 2)	0.20	nsec
exit angle θ (Eq. 6)	0.14	radians
Quarter-turn Collimator		
width	1.27	cm
position X_{max} (Eq. 7)	1.72	cm
radial height ΔX	0.20	cm
angular acceptance $\Delta\theta$ (Eq. 7)	0.10	radians
time spread acceptance Δt (Eq. 9)	0.14	nsec
Electrostatic Field-free Region		
time of flight t (Eq. 8)	2.04	nsec
Deceleration Region		
grid-channel plate separation d	0.16	cm
voltage V	900	volts
approx. time t (Eq. 1)	0.06	nsec
Channel Plate Region		
diameter	1.8	cm
thickness of both plates	0.14	cm
voltage across each plate	900	volts
approx. time	<2	nsec
Anode Region		
Diameter	1.0	cm
channel plate - anode separation d	0.1	cm
voltage	340	volts
time t (Eqs. 5a or 2)	0.18	nsec

Table 2

Time resolutions and efficiencies for alpha particles with different configurations

H(gauss)	1/4 Turn Collimator	Acceleration Grid	FWHM(psec) Uncorr.	Corr.[a]	Pulser	% Eff.
80	Yes	Harp	160	155	95	56
80	Yes	Grid	163	157	83	56
80	No	Harp	175	169	114	58
80	No	Grid	189	183	110	58
50[b]	No	Grid	250	240	100	73
25[b]	No	Grid	490	485	100	75

a) Corrected for energy spread as measured by the Si E detector.

b) Measured with an earlier model of the device which had a 3 cm radius of curvature.

Table 3

Time resolutions,[a] (FWHM) in psec and efficiencies for the final device

Particle	Uncorr.	Corr.[b]	Pulser	% Eff.
104 MeV ^{16}O	90	90	30	95
8.78 MeV ^{4}He	160	155	95	56

a) It was determined that the channel plate discriminator had an electronic "walk" of 50 psec over the amplitude range used in these measurements. No attempt was made to correct the data for this walk.

b) Corrected for energy spread as measured by the Si E detector.

Table 4

Time resolutions (FWHM) in psec for different devices

Device	Particle	Particle	Pulser
CP - E[a]	104-MeV ^{16}O	90[d]	30
45° CP-E[b]	60-MeV ^{16}O	70	50
ΔE - E[c]	60-MeV ^{16}O	70	50

a) Present device.

b) 45° foil and no magnet.

c) 19 μm ΔE

d) Uncorrected for 50 psec walk in the channel plate discriminator.

Figure Captions

Fig. 1. The concept of the secondary electron transport system. The device is placed in a homogeneous magnetic field oriented perpendicular to the plane shown. The three trajectories drawn as solid curves all have the same path length. The off-angle trajectory, shown as the dashed curve, is stopped by the quarter-turn collimator.

Fig. 2. Two views of the mechanical arrangement. The magnet and the block holding the internal parts slide apart.

Fig. 3. A schematic of the electrical arrangement. Two high voltage supplies are used. The acceleration voltage is equal to the foil voltage minus 61% of the channel plate voltage.

Fig. 4. A block diagram of the electronics. PA = pre-amp with both fast and slow outputs. LA = linear amplifier. FA = fast amplifier. CFD = constant fraction discriminator. LGS = fast linear gate and stretcher (EGG #LG105). SCA = single channel analyzer. TAC = time-to-amplitude converter. LG = linear gate.

Fig. 5. Efficiency of obtaining a time-zero signal for alpha particles recorded in the stopping detector as a function of acceleration voltage. a) without the quarter-turn collimator. b) with the quarter-turn collimator.

Fig. 6. Time spectra for monoenergetic alpha particles as a function of the suppression voltage. The satellite peaks become sharper and then disappear with increasing suppression voltage.

Fig. 7. Efficiency of detecting a time-zero signal and the area of the satellite peaks as a function of suppression voltage.

Fig. 8. Pulse height spectra from the channel plates obtained under approximately the same gain conditions with alpha particles and oxygen ions.

Fig. 9. Time spectra showing full widths at half maxima. a) and b) were obtained with the time-zero device for 8.78 MeV alpha particles and 104 MeV oxygen ions, respectively. c) was obtained for 60 MeV oxygen ions using a ΔE-E telescope with a 19 μm thick ΔE detector.

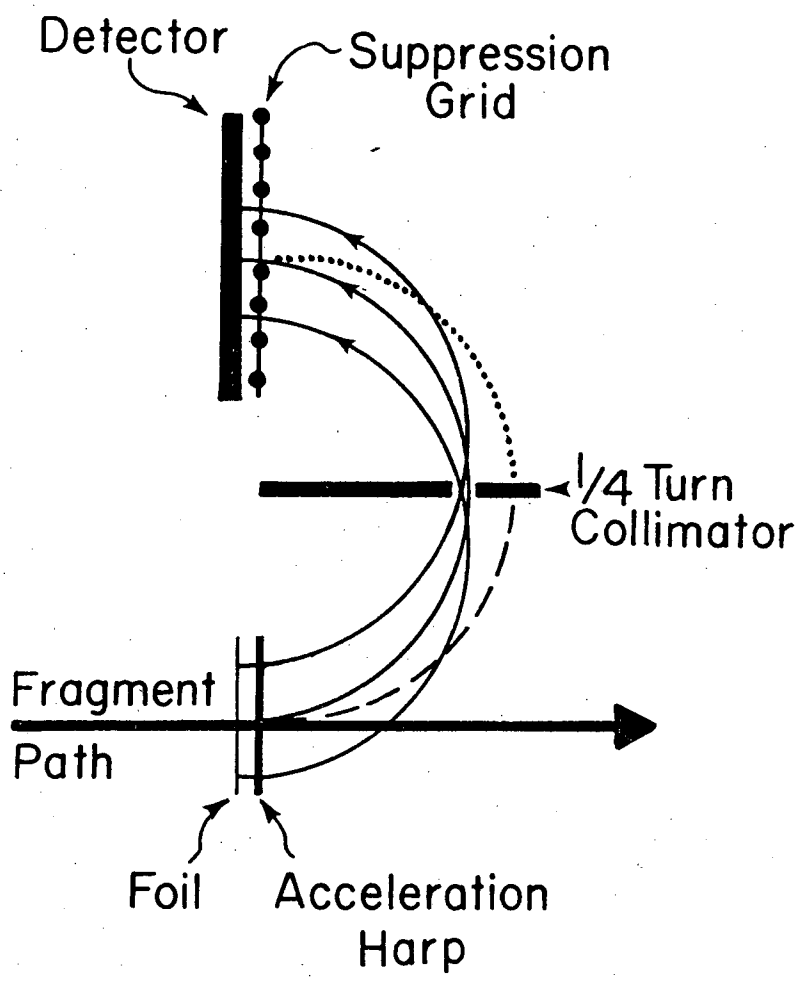

XBL 769-4075

Fig. 1

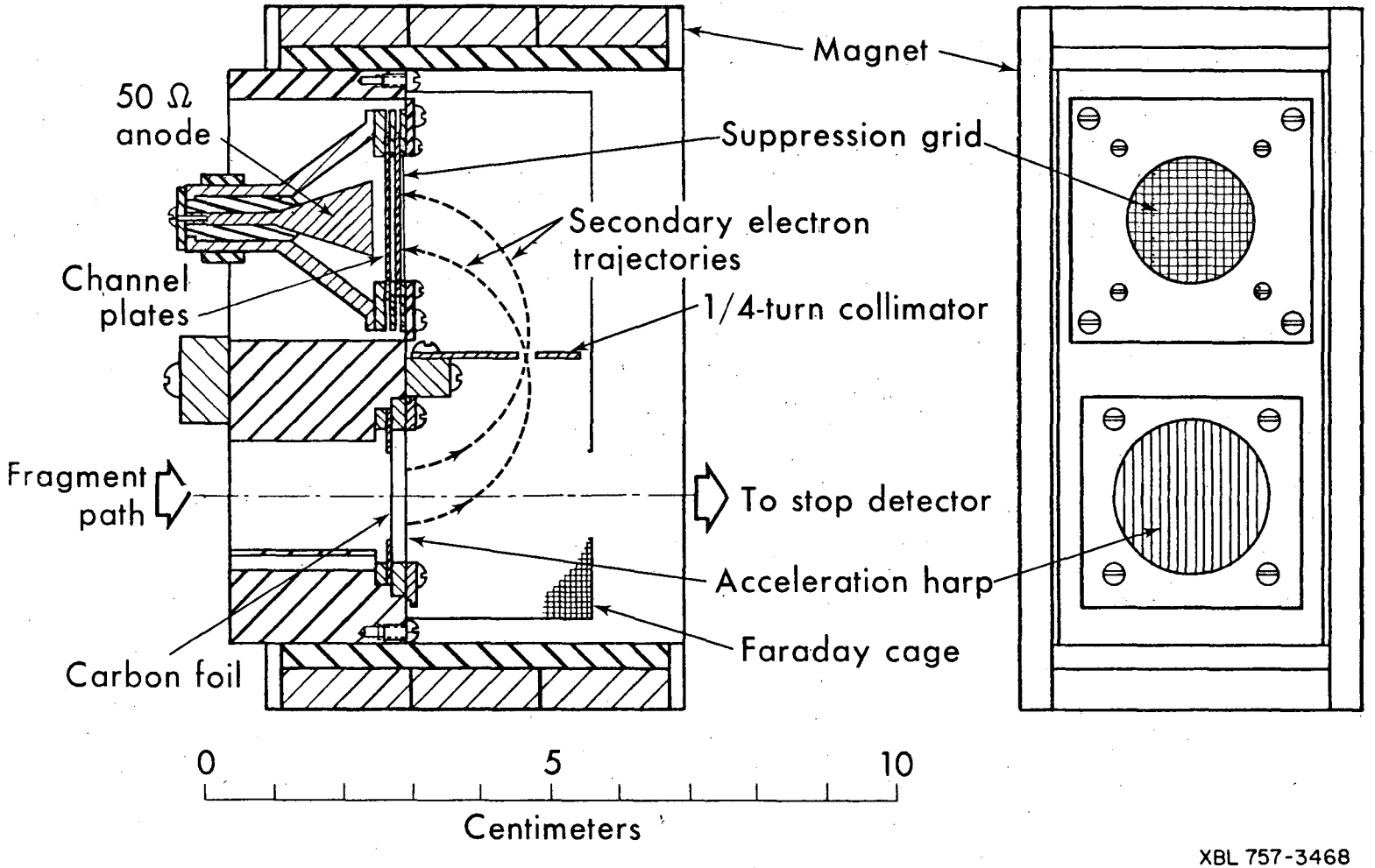

Fig. 2

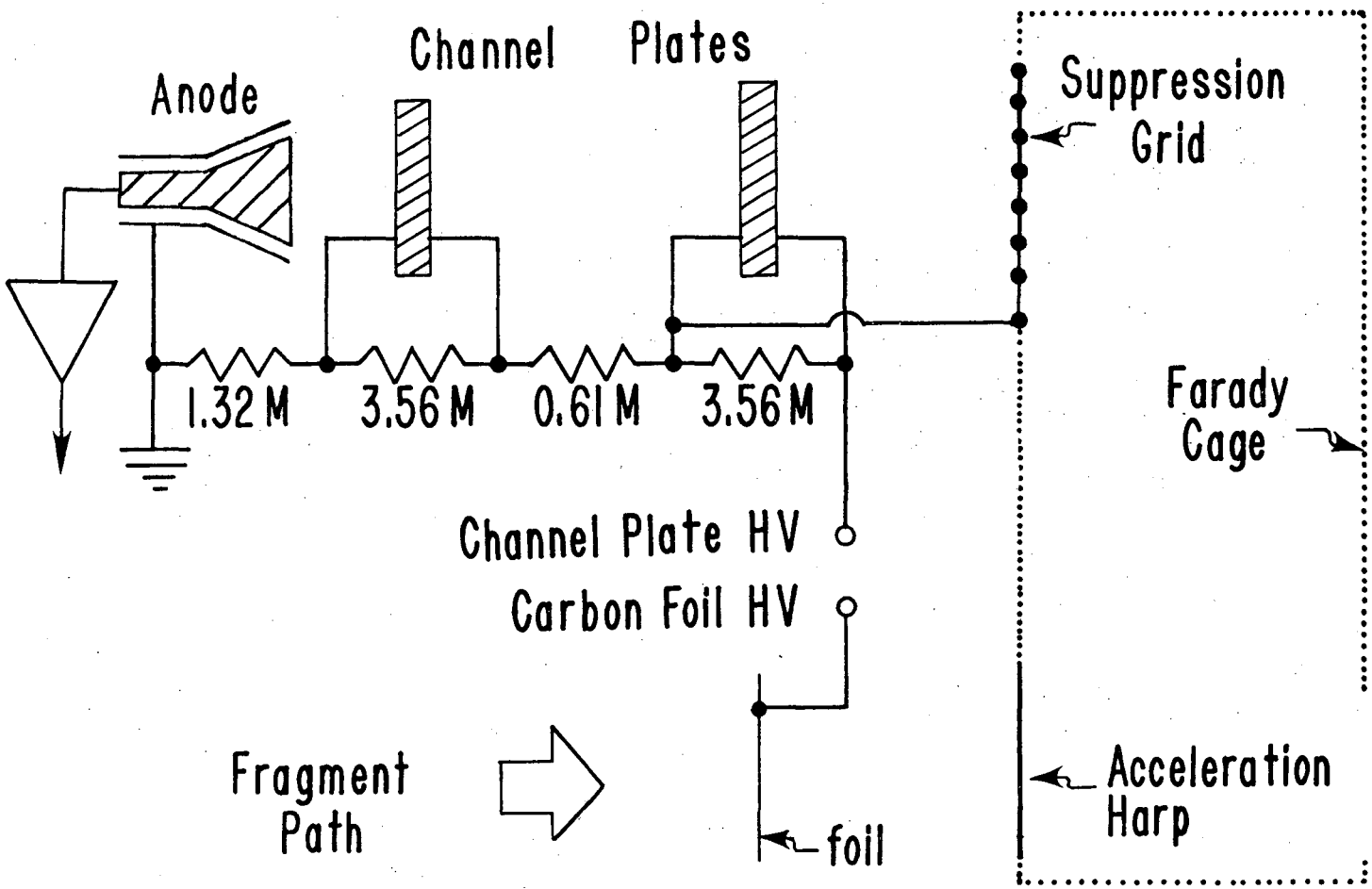

XBL 769-4069

Fig. 3

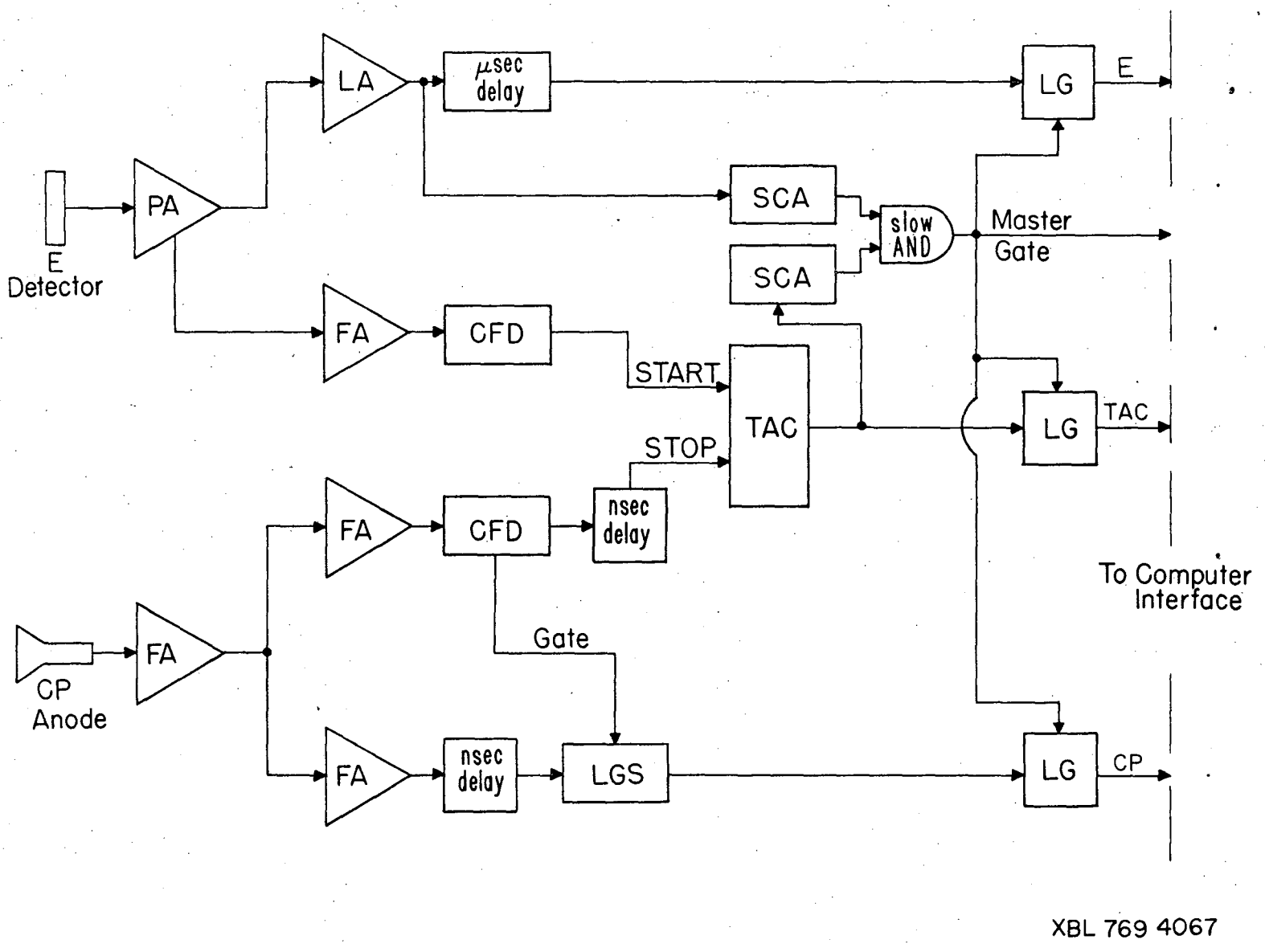

XBL 769 4067

Fig. 4

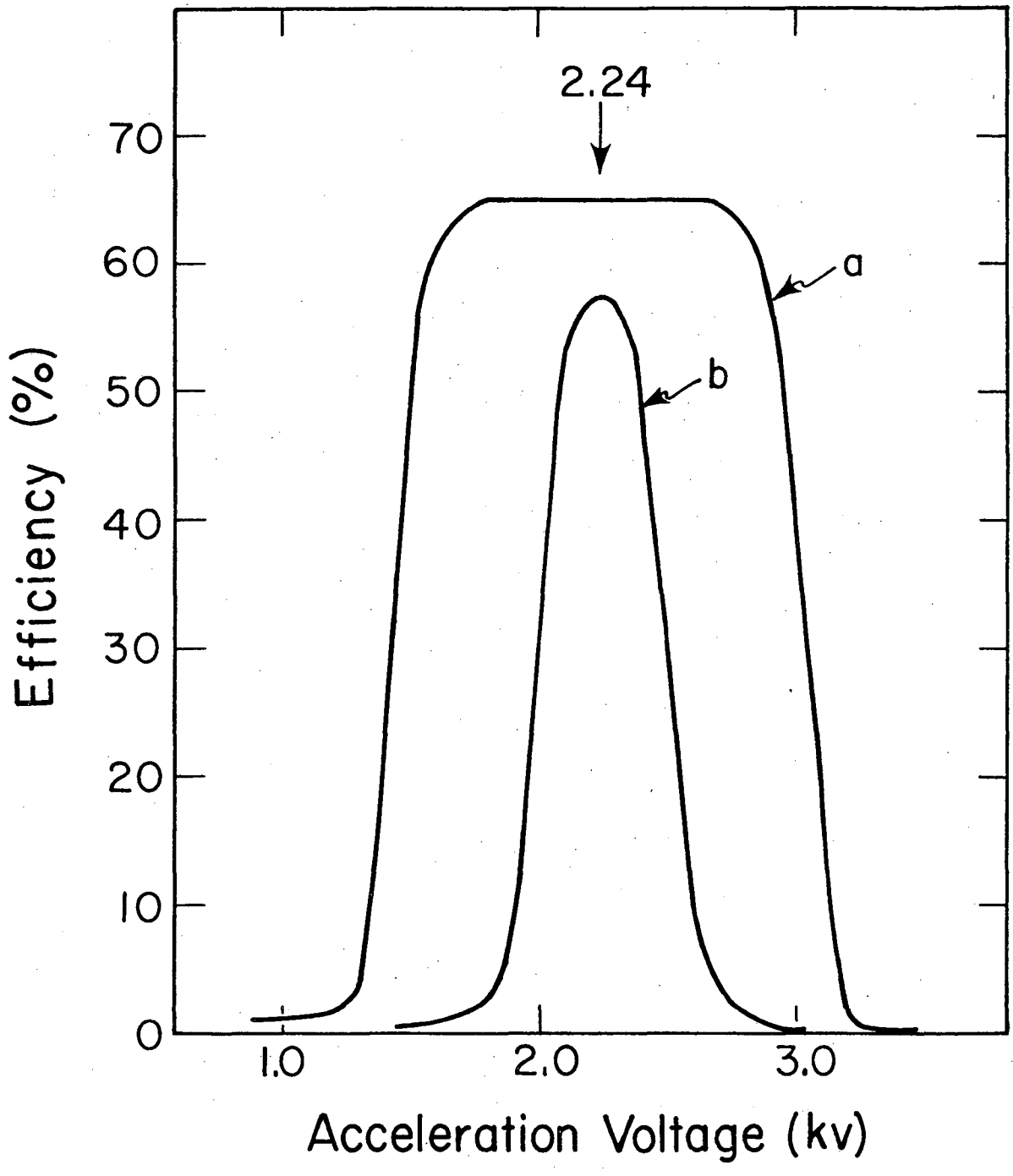

XBL 769-4072

Fig. 5

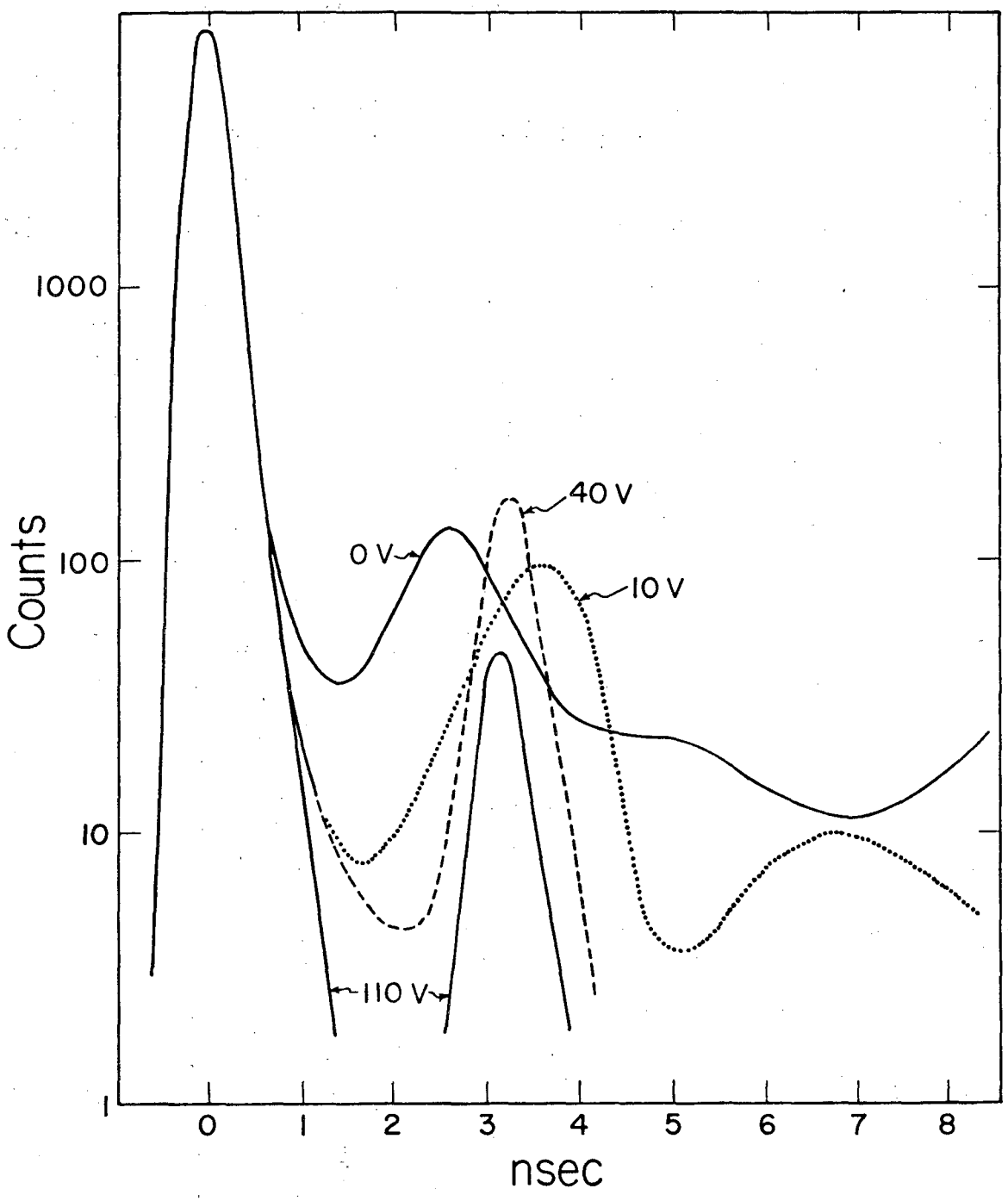

XBL 769-4074

Fig. 6

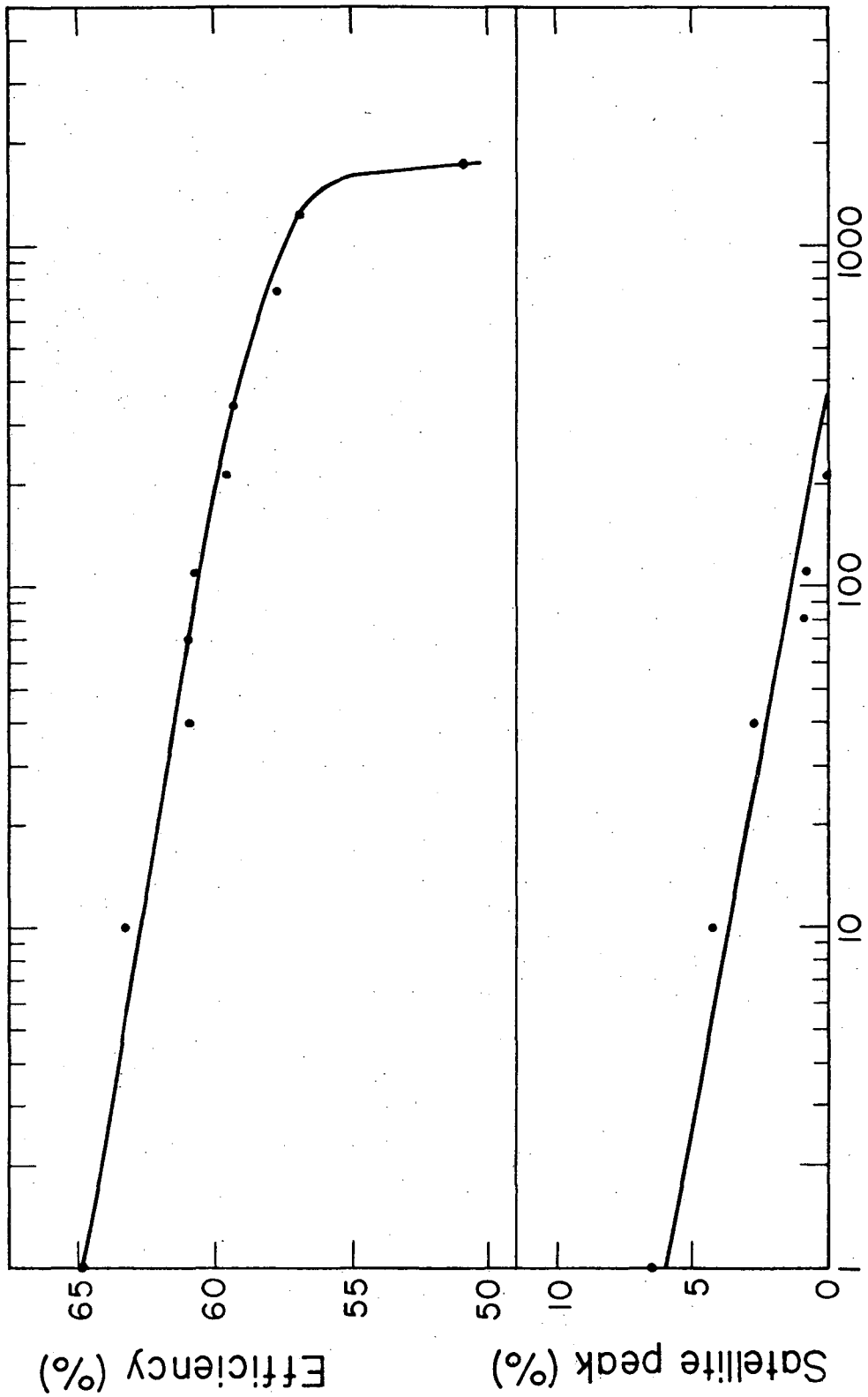

XBL 769-4073

Fig. 7

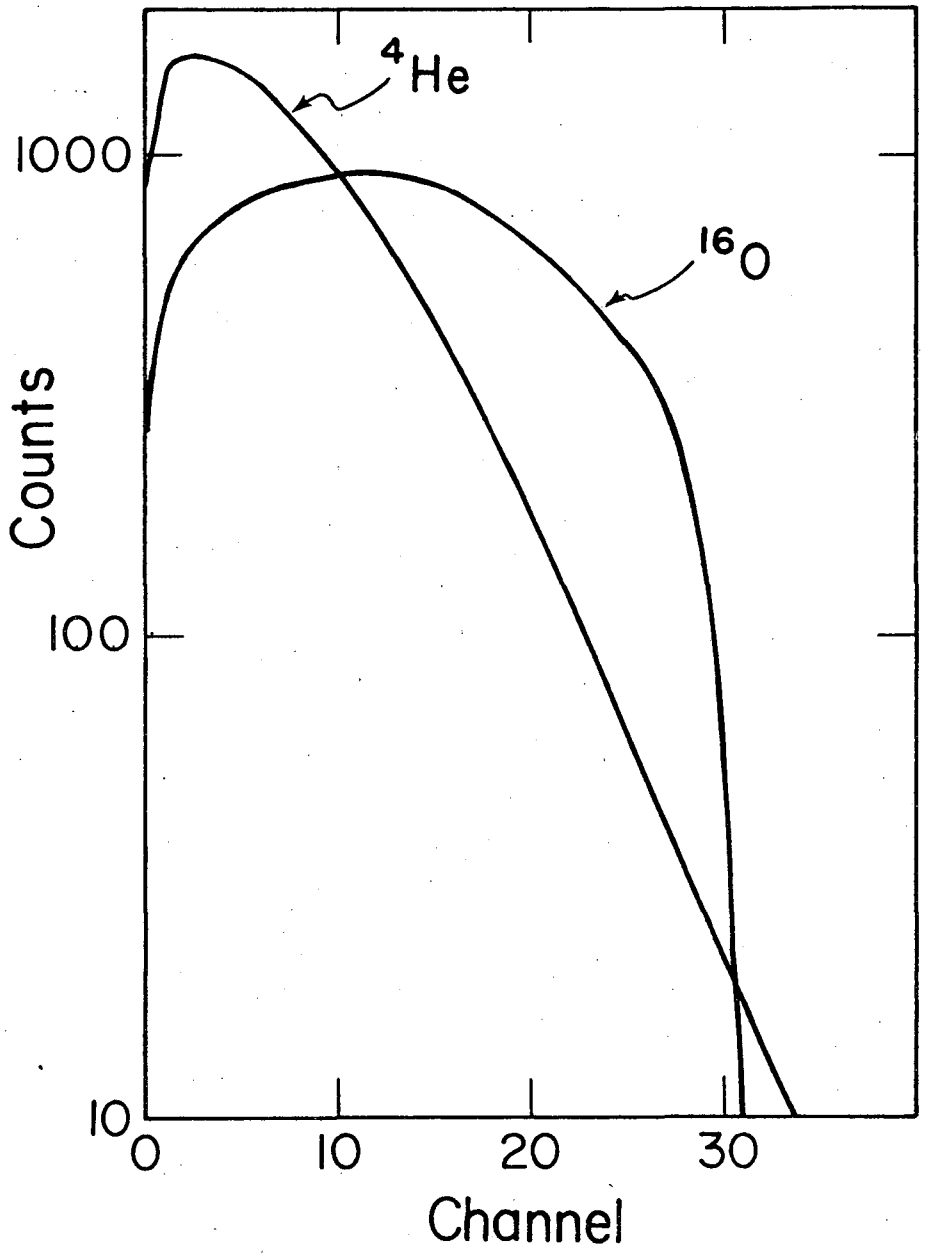

XBL 769-4070

Fig. 8

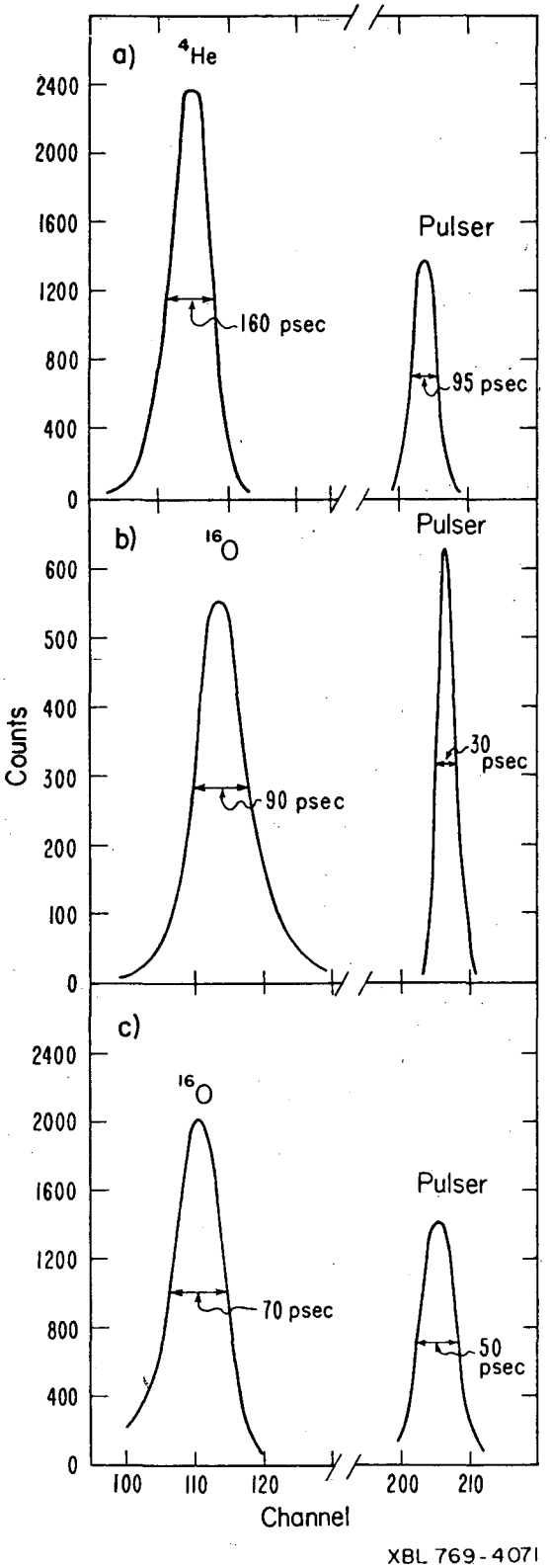
a) ^{4}He
Pulser
160 psec
95 psec
b) ^{16}O
Pulser
90 psec
30 psec
c) ^{16}O
Pulser
70 psec
50 psec
Counts
Channel
XBL 769-4071

Fig. 9

This report was done with support from the United States Energy Research and Development Administration. Any conclusions or opinions expressed in this report represent solely those of the author(s) and not necessarily those of The Regents of the University of California, the Lawrence Berkeley Laboratory or the United States Energy Research and Development Administration.

TECHNICAL INFORMATION DIVISION
LAWRENCE BERKELEY LABORATORY
UNIVERSITY OF CALIFORNIA
BERKELEY, CALIFORNIA 94720